STRUCTURAL BIOLOGY

Single-molecule analysis reveals the mechanism of transcription activation in *M. tuberculosis*

Rishi Kishore Vishwakarma,[1]* Anne-Marinette Cao,[2]* Zakia Morichaud,[1] Ayyappasamy Sudalaiyadum Perumal,[1] Emmanuel Margeat,[2] Konstantin Brodolin[1]†

The σ subunit of bacterial RNA polymerase (RNAP) controls recognition of the −10 and −35 promoter elements during transcription initiation. Free σ adopts a "closed," or inactive, conformation incompatible with promoter binding. The conventional two-state model of σ activation proposes that binding to core RNAP induces formation of an "open," active, σ conformation, which is optimal for promoter recognition. Using single-molecule Förster resonance energy transfer, we demonstrate that vegetative-type σ subunits exist in open and closed states even after binding to the RNAP core. As an extreme case, RNAP from *Mycobacterium tuberculosis* preferentially retains σ in the closed conformation, which is converted to the open conformation only upon binding by the activator protein RbpA and interaction with promoter DNA. These findings reveal that the conformational dynamics of the σ subunit in the RNAP holoenzyme is a target for regulation by transcription factors and plays a critical role in promoter recognition.

INTRODUCTION

The multidrug-resistant forms of *Mycobacterium tuberculosis* (*Mtb*), the pathogen causing human tuberculosis, are a major public health problem worldwide. Development of new antituberculosis therapeutics requires knowledge of the specific regulatory mechanisms of gene expression, which allow *Mtb* to survive antibiotic treatment and thus to cause recurrent infection. The first step of gene expression, transcription initiation, is performed in bacteria by the multisubunit DNA-dependent RNA polymerase (RNAP), which is composed of the catalytic core (subunits $2\alpha\beta\beta'\omega$) and the promoter specificity subunit σ. The σ subunit controls promoter recognition, DNA melting, and initiation of RNA synthesis. All bacteria contain at least one σ subunit, which belongs to the σ^{70} family, and "optional" alternative σ's (*1*). Transcription initiation by the RNAP holoenzyme containing the σ^{70}-family subunit is a spontaneous process driven by the interplay between σ, the RNAP core enzyme, and DNA. Free σ in solution adopts a compact "closed" conformation that is incompatible with promoter DNA binding due to steric occlusion of its promoter-binding domains, σ2 and σ4 (*2–4*). Ensemble luminescence resonance energy transfer (LRET) studies demonstrated that, during assembly of the RNAP holoenzyme, σ undergoes a core-induced conformational change involving repositioning of the σ2 and σ4 domains (*5–7*). As a result, σ adopts an "open" conformation, observed in the crystal structures of the RNAP holoenzyme, where domains σ2 and σ4 contact a coiled-coil region of the β' subunit (β'CC) and the β subunit flap domain (β-Flap), respectively, and the distance between σ2 and σ4 domains matches the distance between the −10 and −35 promoter elements (*8, 9*). To initiate transcription, RNAP first forms an unstable "closed complex" (RPc) with the promoter, which isomerizes into a transcriptionally competent "open complex" (RPo) (*10*). Recent studies demonstrated that RNAP of *Mtb* (*Mtb*RNAP) differs from RNAP of the paradigm bacteria, *Escherichia coli* (*Eco*RNAP), because it requires an accessory RNAP-binding protein, RbpA, to form stable RPo (*11–13*). The nature of this factor dependency remains unknown. RbpA in *Mtb* is an essential protein that interacts with σ2 domain and stimulates transcription initiation by *Mtb*RNAPs containing either the principal

σ^A or the stress-response σ^B subunit (*12, 14*). It is implicated in control of the pathogen physiological states and likely in the development of latent tuberculosis (*15, 16*).

Here, we used single-molecule Förster resonance energy transfer (smFRET) to explore the molecular basis for RbpA requirement by *Mtb*RNAP. We compared conformational states of the principal σ subunit of *E. coli*, σ^{70}, and the σ^B subunit of *Mtb* in solution, upon RNAP holoenzyme assembly and promoter binding. σ^B differs from σ^{70} by the lack of the N-terminal autoinhibition domain σ1.1 and the lack of the nonconserved domain (NCD) (Fig. 1A). The promoter-binding domains of both σ subunits display high structural similarity and can recognize identical promoter consensus elements (*12*). We show that σ^{70} and σ^B subunits exist in open and closed states even after binding to their lineage-specific RNAP core. However, *Mtb* σ^B remains preferentially in the closed conformation unless it is stabilized in the open conformation by binding of RbpA and promoter DNA.

RESULTS AND DISCUSSION

The σ^{70} subunit in the *Eco*RNAP holoenzyme undergoes conformational fluctuations

To probe σ conformation, we monitored distances between donor and acceptor fluorescent probes introduced in domains σ2 and σ4. The σ^{70} derivative with cysteines (Cys) at positions 442 and 579 and the σ^B derivative with Cys at positions 151 and 292 (corresponding to positions 440 and 581 in σ^{70}, respectively) were randomly labeled with DY-547 (donor) and DY-647 (acceptor) fluorescent probes (Fig. 1, A and B, and fig. S1). Previous studies (*5–7*) and control experiments demonstrated that the modifications did not significantly affect σ activities such as holoenzyme assembly, promoter binding, and promoter melting but displayed quantitative defects in run-off transcription (fig. S2). Note that we performed all biochemical assays [transcription, KMnO$_4$ probing, and electrophoretic mobility shift assay (EMSA)] in the hundred nanomolar protein concentrations range, with a threefold excess of the σ subunit and RbpA over the RNAP core.

To perform the smFRET measurements, we used confocal optical microscopy with pulsed interleaved laser excitation and multiparameter fluorescence detection (PIE-MFD) (*17, 18*). This setup allowed monitoring distances between fluorescent probes in single σ molecules diffusing in solution, either free or in complex with ligands (RbpA,

[1]Institut de Recherche en Infectiologie de Montpellier, CNRS, Université de Montpellier, Montpellier, France. [2]Centre de Biochimie Structurale, CNRS, INSERM, Université de Montpellier, Montpellier, France.
*These authors contributed equally to this work.
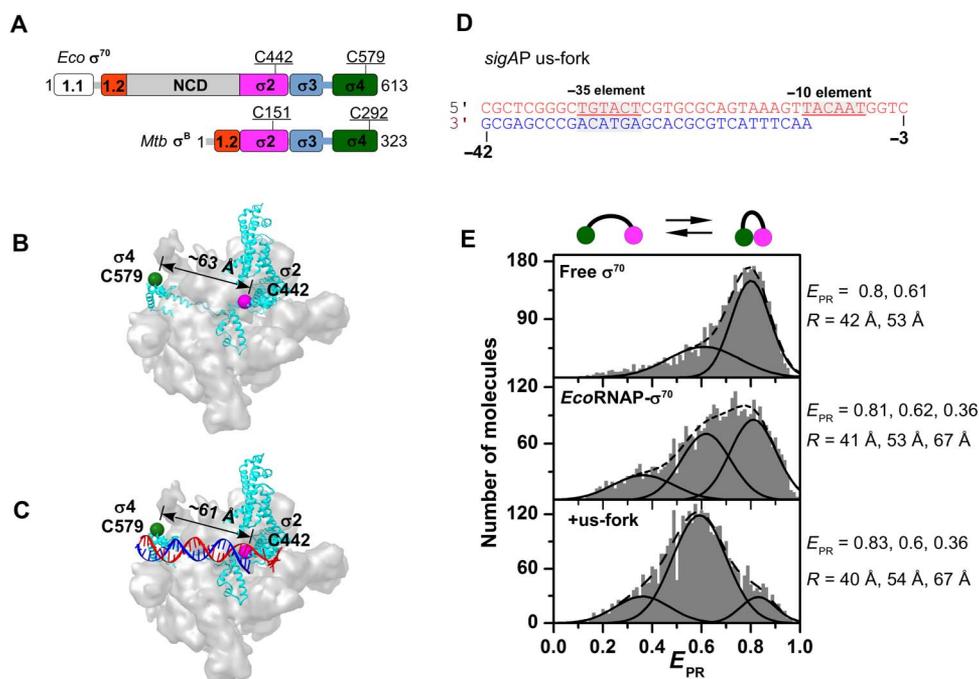†Corresponding author. Email: konstantin.brodolin@inserm.fr

Fig. 1. The σ70 subunit in the RNAP holoenzyme exhibits conformational heterogeneity. (**A**) Scheme of the σ subunits. Positions of the Cys substitutions are underlined. (**B**) Structure of the EcoRNAP-σ70 holoenzyme [Protein Data Bank (PDB) code: 4IGC (35)] and (**C**) its complex with us-fork. The subunits of the RNAP core are shown as molecular surfaces, and the σ subunit is shown as ribbons in cyan. The Cα atoms of the σ subunit residues labeled by fluorophores are shown as spheres in green (σ domain 4) and magenta (σ domain 2). The distance between the Cα atoms is indicated. (**D**) Sequence of the us-fork DNA. The −10 and −35 promoter elements are underlined and shaded. (**E**) E_{PR} histograms for free σ70, EcoRNAP-σ70 holoenzyme, and its complex with us-fork (+us-fork). Two conformations of σ, corresponding to the open and closed states, are shown schematically on the top. The black thick lines show Gaussian fits of smFRET efficiencies for individual subpopulations, and the dashed lines represent the sum of Gaussians for the overall population. Mean peak E_{PR} and R are shown on the right.

RNAP core, and/or DNA). The smFRET measurements, which necessitate low picomolar concentrations of the labeled σ subunit, were performed with the ~10^4-fold excess of the core RNAP and RbpA over σ to ensure maximum efficiency of the holoenzyme formation. Only molecules labeled with both donor and acceptor were selected for calculation of their apparent and corrected FRET efficiencies (E_{PR} and E) and donor-acceptor distances (R) (figs. S1E and S4).

First, we compared donor-acceptor distances in the free σ70 subunit with that in the EcoRNAP-σ70 holoenzyme (Fig. 1E). Free σ70 displayed asymmetric distribution of E_{PR} values that can be fitted with two overlapping Gaussians. The main peak ($E_{PR} = 0.8$) corresponds to the donor-acceptor distance, R ~ 42 Å, which is in good accordance with those (36 to 42 Å) obtained in ensemble LRET experiments (table S1) and supports the view that free σ70 preferentially adopts a compact, closed, conformation (4, 5). However, the presence of the second peak ($E_{PR} = 0.61$) indicates that free σ70 undergoes conformational fluctuations, moving apart (opening) and moving together (closing) of the σ2 and σ4 domains, on a time scale longer than milliseconds (our observation time).

Binding of σ70 to the EcoRNAP core is expected to induce an ~20 Å increase in the donor-acceptor distance (table S1) (5–7). After the addition of the EcoRNAP core, σ70 exhibited a broad distribution of FRET efficiencies that can be fitted to three Gaussians corresponding to three subpopulations of molecules. Two subpopulations, with $E_{PR} = 0.62$ and 0.36, correspond to open conformations of σ70 with a 10 and 25 Å increase in interdomain distance, respectively. However, 40% of σ70 molecules still adopted a closed conformation ($E_{PR} = 0.81$) despite being bound to the EcoRNAP core, as demonstrated by species-

specific fluorescence correlation spectroscopy (ssFCS) (fig. S5C) (19). We conclude that the open conformation of σ70 in the EcoRNAP holoenzyme is not stable and remains in equilibrium with the closed conformation.

Promoter binding should stabilize the open conformation of the σ subunit (Fig. 1C). We thus tested EcoRNAP-σ70 interaction with the synthetic fork junction DNA template (us-fork), derived from the sigAP promoter (Fig. 1D) for which RNAP can efficiently form RPo-like complexes even at suboptimal temperatures (22°C in our case) (20). Upon us-fork binding, the fraction of molecules at $E_{PR} = 0.6$ (R = 54 Å) is increased to 71%, which suggests that interaction with −10 and −35 elements of the promoter stabilizes σ70 in the open conformation. Thus, in the promoter-bound RNAP-σ70 holoenzyme, the donor-acceptor distance was found to be 11 Å greater than that in σ70 adopting a closed conformation (table S2). The minor high FRET ($E_{PR} = 0.83$; ~11% of molecules) and low FRET subpopulations ($E_{PR} = 0.36$; ~18% of molecules), still observed in the presence of DNA, likely correspond to the unbound EcoRNAP holoenzyme.

The σB subunit in the MtbRNAP holoenzyme retains closed conformation

In the next set of experiments, to explore whether this unexpected conformational heterogeneity observed in the E. coli RNAP holoenzyme is conserved in Mtb, we monitored conformational changes in the σB subunit (Fig. 2). Free σB exhibited a bimodal distribution of E_{PR} values similar to the one observed for free σ70 with $E_{PR} = 0.83$ (72% of molecules) and 0.67 (28% of molecules) (Fig. 2A). Addition of RbpA, which can bind free σB in solution (12, 14, 21), resulted in a strong
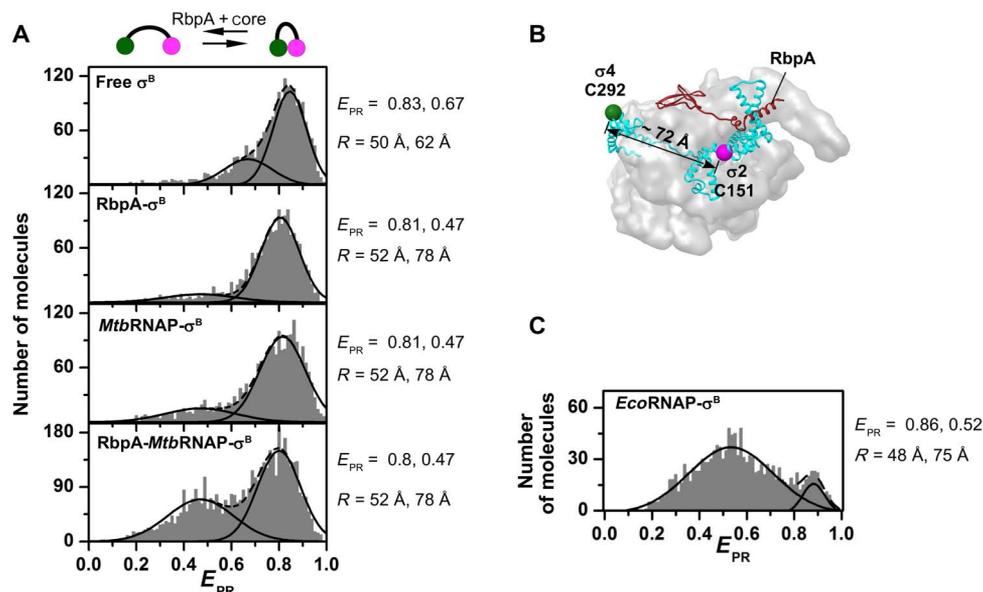
Fig. 2. RbpA is required for "opening" of σ^B in the MtbRNAP holoenzyme. (**A**) E_{PR} histograms for free σ^B, RbpA-σ^B complex, and MtbRNAP-σ^B and RbpA-MtbRNAP-σ^B complex. (**B**) Structure of *Mycobacterium smegmatis* RNAP in complex with RbpA [PDB code: 5TW1 (*22*)]. Labeling as in Fig. 1B. Residue numbering corresponds to the σ^B subunit. (**C**) E_{PR} histogram of chimeric EcoRNAP-σ^B holoenzyme.

reduction of the peak at $E_{PR} = 0.67$, indicating that RbpA binding can restrain σ^B conformational dynamics. Surprisingly, binding of σ^B to the MtbRNAP core had little effect on E_{PR} distribution (Fig. 2A). Only a minor subpopulation of molecules (20%) displayed the FRET efficiency expected for the open σ^B conformation ($E_{PR} = 0.47$). The ssFCS analysis confirmed that the major subpopulation, at $E_{PR} = 0.81$, corresponds to σ^B bound to the MtbRNAP core (fig. S5, A and B). Thus, we conclude that, in the MtbRNAP holoenzyme, most of the σ^B molecules remained in a closed conformation characteristic of free σ^B. Addition of RbpA to MtbRNAP-σ^B holoenzyme resulted in a strong increase of the peak at $E_{PR} = 0.47$ (Fig. 2A), showing that binding of RbpA to MtbRNAP-σ^B partially stabilizes an open conformation of σ^B with a donor-acceptor distance that is ~24 Å greater than that observed in free σ^B. The fact that a subpopulation of MtbRNAP-σ^B containing σ^B in a closed state ($E_{PR} = 0.8$) was still observed in the presence of RbpA likely reflects an equilibrium between RbpA-bound and free MtbRNAPs. The calculated donor-acceptor distance in MtbRNAP-σ^B ($R = $ ~78 Å) was in the range of the distances observed in structures of the RNAP holoenzyme (table S3). Because MtbRNAP was poorly active in transcription initiation without RbpA (*11*, *12*), we supposed that MtbRNAP activity depends on the ability of σ^B to adopt an open state, with the distance between $\sigma2$ and $\sigma4$ domains optimal for promoter recognition. To test this hypothesis, we used a chimeric holoenzyme, reconstituted from σ^B and EcoRNAP core, which has been shown to form a stable promoter complex without RbpA (*12*). Accordingly, smFRET analysis performed on EcoRNAP-σ^B (Fig. 2C) demonstrated that most σ^B molecules adopt an open conformation with $E_{PR} = 0.52$. A minor subpopulation of σ^B molecules (~15%) displayed high FRET efficiency ($E_{PR} = 0.86$) that likely corresponds to free σ^B or a residual fraction of σ^B retaining the closed conformation in the holoenzyme. Thus, we conclude that the chimeric enzyme was active in promoter binding because the EcoRNAP core is able to stabilize the open conformation of σ^B, whereas MtbRNAP lacks this potency in the absence of RbpA.

RbpA and promoter DNA stabilize the open conformation of σ^B

Next, we examined the impact of us-fork binding on σ^B conformation in the MtbRNAP holoenzyme (Fig. 3). The MtbRNAP holoenzyme containing labeled σ^B (Dy-σB) was tested for its ability to bind unlabeled us-fork in the EMSA. MtbRNAP containing unlabeled wild-type σ^B was used as a control in EMSA with the Cy3-labeled us-fork (Fig. 3B). Holoenzymes containing either unlabeled or labeled σ^B formed detectable stable competitor-resistant complexes with us-fork. Complex formation was stimulated by RbpA $\approx$ 2.5- to 5-fold (for unlabeled and labeled σ^B, respectively; Fig. 3C), suggesting that RbpA stabilizes RPo but is not essential for promoter binding in conditions when promoter melting is bypassed. On the contrary, RbpA was essential for stable complex formation on the full-length homoduplex DNA *sigA*P promoter (*12*). We conclude that, in the absence of RbpA, MtbRNAP forms unstable promoter complexes because σ^B tends to adopt a closed conformation inappropriate for binding to −10 and −35 elements. Accordingly, chimeric EcoRNAP-σ^B, which contains σ^B in open conformation (Fig. 2C), formed competitor-resistant complexes with us-fork as efficiently as the RbpA-MtbRNAP-σ^B complex (Fig. 3B).

Binding of us-fork to MtbRNAP-σ^B resulted in the appearance of the subpopulation of σ^B in an open conformation ($E_{PR} = 0.41$) that became prevalent (Fig. 3D). In agreement with the stabilization effect of RbpA in EMSA, its addition increased the fraction of σ^B in the open conformation at the expense of the closed state ($E_{PR} = 0.81$) (Fig. 3D). Control experiments performed on the us-fork labeled with the black hole quencher (BHQ2) (fig. S6) demonstrated that only the subpopulation at $E_{PR} = 0.41$ corresponds to DNA-bound MtbRNAP-σ^B, whereas the subpopulation at $E_{PR} = 0.81$ corresponds to unbound MtbRNAP-σ^B species. The difference in E_{PR} values between promoter-bound MtbRNAP-σ^B ($E_{PR} = 0.41$) and MtbRNAP-σ^B in complex with RbpA ($E_{PR} = 0.47$) (Fig. 2A) likely reflects a shift in the mean dye
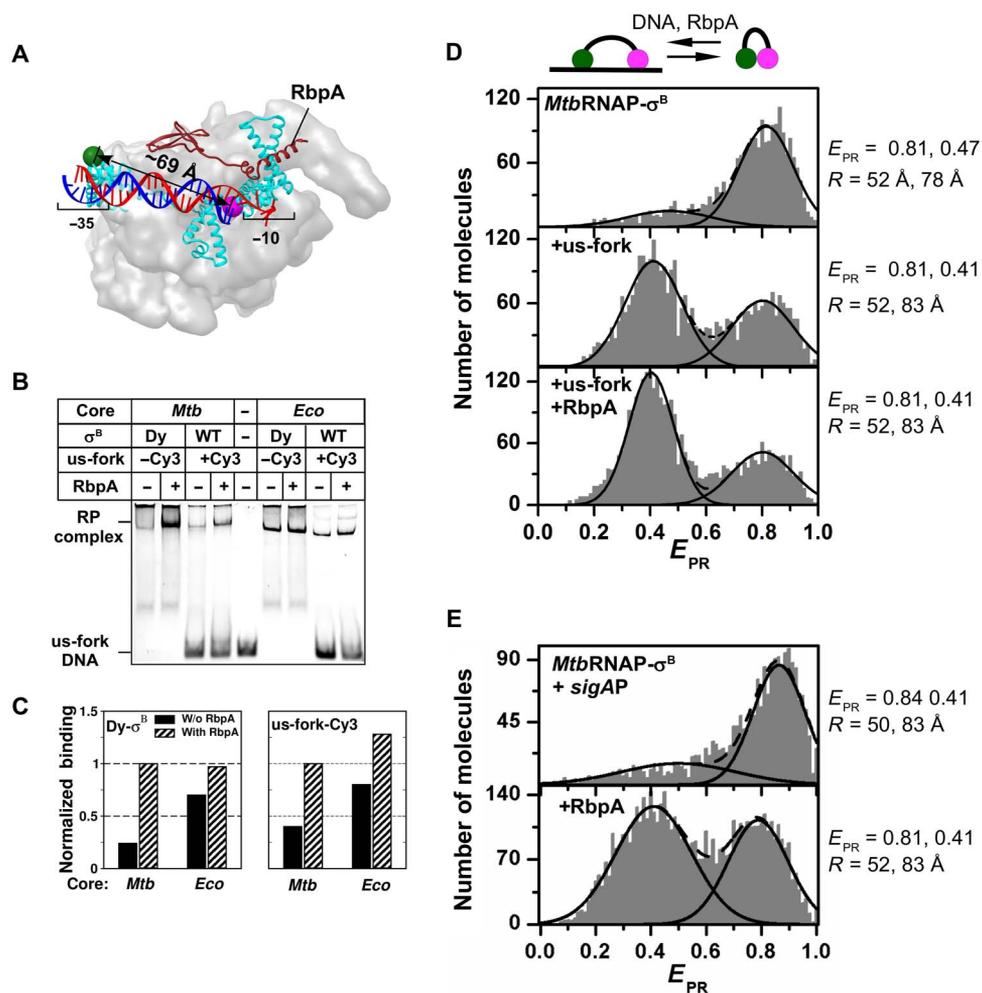
Fig. 3. Interaction with promoter DNA stabilizes the open conformation of the σ^B subunit. (**A**) Structure of *M. smegmatis* RNAP in complex with RbpA and us-fork (blue, template strand; red, nontemplate strand) (PDB code: 5TW1). (**B**) Native gel electrophoresis analysis of the promoter complex formation between labeled (+Cy3) and unlabeled (−Cy3) us-fork DNA and RNAP holoenzymes containing σ^B [wild-type (WT)] and donor-acceptor–labeled σ^B (Dy). (**C**) Quantification of the gel shown in (B). Values were normalized to that obtained for *Mtb*RNAP-σ^B in the presence of RbpA. (**D**) E_{PR} histograms for *Mtb*RNAP-σ^B in complex with us-fork without (+us-fork) or with RbpA (+us-fork + RbpA). (**E**) E_{PR} histograms for *Mtb*RNAP-σ^B in complex with *sigA*P promoter without (+*sigA*P) or with RbpA (+RbpA).

positions due to steric clash with DNA (fig. S4, D and E). We conclude that RbpA and us-fork act cooperatively to stabilize σ^B in open conformation, as found in RNAP structures. RbpA, which inserts between σ2 and σ4 domains (Fig. 3A) (*22*), stabilizes promoter complexes by preventing the collapse of σ^B to the closed state and additionally bridging us-fork and RNAP through protein-DNA contacts (*13*). Interaction of σ^B with promoter elements also hinders transition to the closed state.

Finally, we explored whether binding of *Mtb*RNAP to the 106–base pair (bp) *sigA*P promoter homoduplex DNA also favors the formation of the open σ^B conformation in the *Mtb*RNAP holoenzyme (Fig. 3E). Unlike the us-fork, the *sigA*P promoter had no effect on the distribution of E_{PR} values, which remained similar to that observed for free holoenzyme. Thus, we conclude that *Mtb*RNAP was unable to form a stable complex with the *sigA*P promoter, in agreement with the published EMSA and deoxyribonuclease I footprinting results (*12*). We only observed the low FRET peak with $E_{PR} = 0.41$ in the presence of RbpA (Fig. 3E, panel +RbpA). This peak is a hallmark of the open σ^B conformation found in the RPo-like complex of *Mtb*RNAP with us-fork (Fig. 3D). The

ratio between high FRET (unbound *Mtb*RNAP) and low FRET (bound *Mtb*RNAP) subpopulations was shifted toward high FRET, as compared to the distribution of E_{PR} values observed in the presence of us-fork. The discrepancy between the results obtained with us-fork and the promoter fragment is expected, because smFRET data acquisition was performed at 22°C, a temperature that is suboptimal for promoter melting and RPo formation (*10*). Thus, the equilibrium was shifted toward unstable closed promoter complexes (RPc) and dissociation of *Mtb*RNAP from the promoter. The us-fork complex formation does not need the DNA melting step and is therefore largely temperature-independent (*20*).

It has been shown that binding of RNAP to the "extended −10" class promoter does not require interaction between the σ4 and the −35 element (*23*) and does not require an open conformation of σ (*24*). Our model predicts that *Mtb*RNAP should form a stable complex with the extended −10 promoter in the absence of RbpA. To test this prediction, we used a derivative of the *sigA*P us-fork that harbors the extended −10 motif and lacks the −35 element (fig. S5A). The EMSA assay demonstrated that *Mtb*RNAP efficiently binds the extended −10 us-fork in the
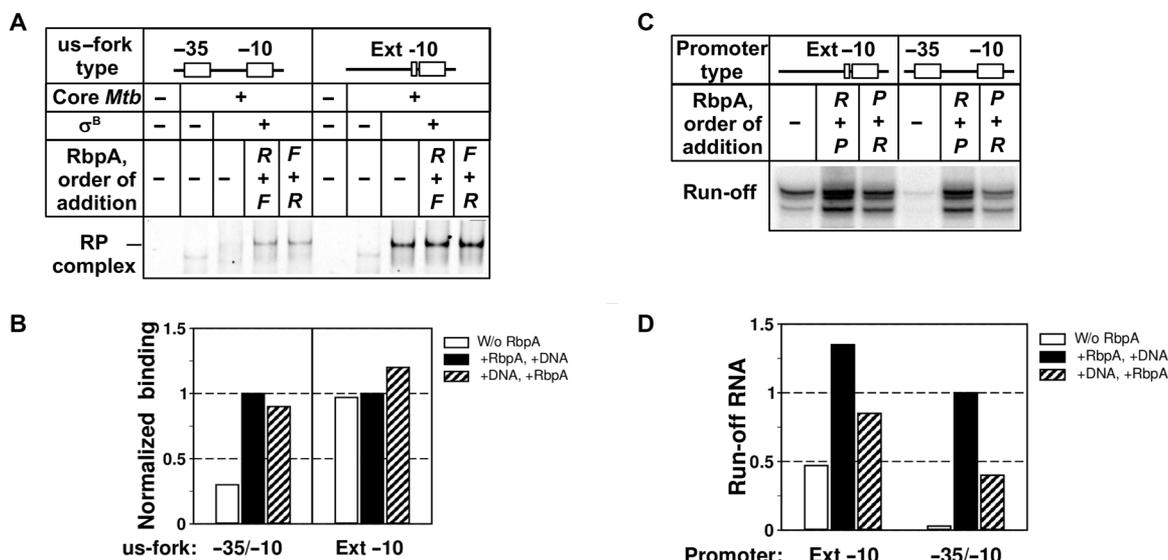
Fig. 4. Effect of promoter architecture on *Mtb*RNAP activity. (**A**) Native gel electrophoresis analysis of the *Mtb*RNAP complex formation with Cy3-labeled us-fork and us-fork harboring extended −10 element (Ext −10). RbpA was added either before (R + F) or after (F + R) the us-fork DNA. (**B**) Quantification of the gel shown in (A). Values were normalized to that obtained in the presence of RbpA for each template separately. (**C**) Run-off [³²P]RNA products synthesized in multiple-round transcription from the wild-type *sigA*P promoter and its derivative harboring extended −10 element. (**D**) Quantification of the RNA products shown in (C). Values were normalized to that obtained for the wild-type *sigA*P promoter in the presence of RbpA. RbpA was added either before (R + P) or after (P + R) the promoter DNA.

absence of RbpA (Fig. 4, A and B). The experiment was performed using different orders of RbpA addition to test whether the activator can stabilize preformed *Mtb*RNAP-DNA complexes. Addition of RbpA had no effect on binding of the *Mtb*RNAP to the extended −10 us-fork. The complex of *Mtb*RNAP with the wild-type *sigA*P us-fork was stabilized irrespective of the order of RbpA addition. To determine whether RbpA is also dispensable for transcription initiation at the extended −10 promoter, we performed a run-off transcription assay using the *sigA*P promoter derivative harboring the extended −10 motif (Fig. 4, C and D). In agreement with the result of EMSA, *Mtb*RNAP was able to initiate transcription from the extended −10 promoter without RbpA. However, RbpA stimulates transcription even at the extended −10 promoter, likely through direct interaction with DNA as reported before (*13*, *22*). RbpA activates *Mtb*RNAP less efficiently when added to the reaction together with nucleotide triphosphates (NTPs) after the incubation of *Mtb*RNAP with promoter DNA. This order-of-addition effect likely reflects slow kinetics of RPo formation on the *sigA*P promoter and not the interference between DNA and RbpA upon *Mtb*RNAP binding. In support of this idea, no order-of-addition effect of RbpA was observed upon binding of *Mtb*RNAP to us-fork. On the basis of the above results, we propose two pathways of RbpA loading to the promoter complex and *Mtb*RNAP activation: direct binding to free *Mtb*RNAP and binding to preformed promoter complex (see model in Fig. 5). However, we cannot exclude that activation involves dissociation of *Mtb*RNAP from the promoter, its association with RbpA, and following rebinding in an active form.

The results of our study establish that σ subunits in RNAP holoenzymes can adopt different conformational states and that the capacity of the RNAP core to stabilize the σ open state varies between bacterial species. The conformational flexibility of σ in RNAP likely originates from the conformational flexibility of the RNAP core, for example, movement of the β′ clamp and β-flap domains (*24*–*26*) and/or partial disruption of the σ-core contacts. This conformational flexibility of the vegetative σ subunits may allow RNAP to adapt to a large spectrum of
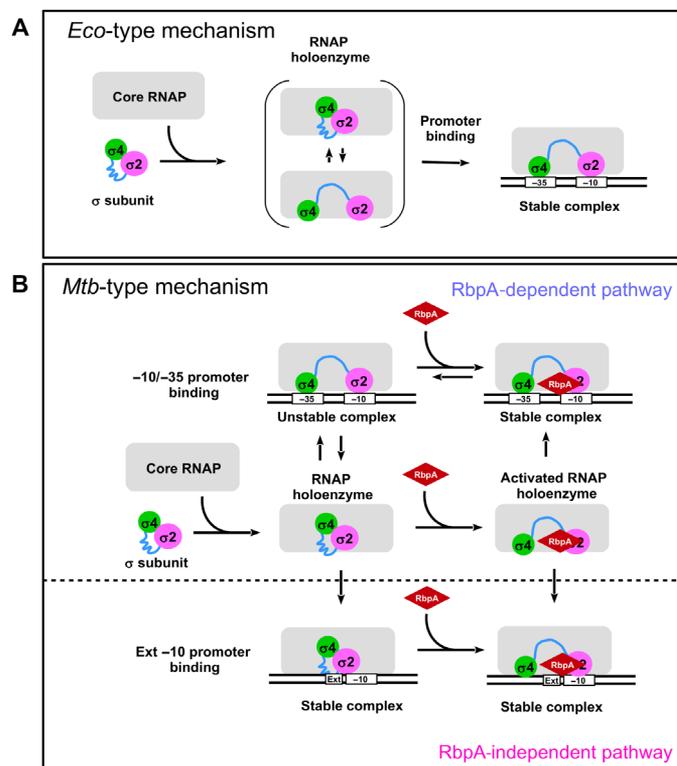

Fig. 5. The "dynamic" model for the σ subunit activation and promoter recognition. (**A**) Activator-independent mechanism used by *E. coli* RNAP. (**B**) Activator-dependent and activator-independent mechanisms used by *Mtb*RNAP.

promoter architectures. RbpA and other RNAP-binding transcriptional factors can control RNAP activity by switching σ between open/closed states. In support of this model, the crystal structure of the *Thermus thermophilus* RNAP with the phage protein gp39 revealed the σ^A

subunit in a closed conformation with a ~33 Å distance between domains σ2 and σ4 (*24*). We speculate that the intrinsic tendency of σ to adopt closed conformations plays a critical role in the process of RPo formation at the −10/−35–type consensus promoters but not at the extended −10–type promoters (Fig. 5). Because most *Mtb* promoters lack a pronounced −35 motif (*27*), stabilization of the σ open conformation by RbpA is required to compensate the weak interactions at the −35 element and favor RPo formation.

MATERIALS AND METHODS
Proteins and DNA templates
Recombinant *Mtb* and *E. coli* RNAP core enzymes, σ subunits, and RbpA protein were expressed and purified as described (*12*, *28*). Fork junction DNA templates were prepared by annealing of two oligonucleotides corresponding to template and nontemplate DNA strands of the *sigA*P promoter from *Mtb* (Fig. 1D) (*29*). The 106-bp *sigA*P promoter DNA fragment (spanning positions −56 to +50) was prepared as described (*12*). The *sigA*P derivative harboring the sequence 5′-TGTG-3′ at positions −17 to −14 and substitutions −30A→G; −31T→C; −33T→C was prepared by annealing of two synthetic oligonucleotides and amplification using *sigA*P-specific primers (*12*). The substitutions Thr^{151}→Cys and Gly^{292}→Cys in σ^B and the substitution Gln^{579}→Cys in σ^{70} were constructed using a site-directed mutagenesis kit (Agilent Technologies). To construct double-Cys mutant of σ^{70}, we used a pET28 plasmid encoding a single Cys derivative of σ^{70}, Cys^{442}, provided by R. Gourse (*30*).

Labeling of the σ^B and σ^{70} subunits
Protein labeling was performed as described by Kim *et al.* (*31*), with modifications. Purified σ subunit (500 μg) dissolved in 1 ml of reduction buffer [20 mM tris-HCl (pH 7.9), 200 mM NH$_4$Cl, 2.5 mM EDTA, 0.2% Triton X-100, and 10 mM dithiothreitol (DTT)] was incubated for 2 hours at 4°C. Solid (NH$_4$)$_2$SO$_4$ powder was added to the sample to 70% of saturation and gently agitated until dissolved. The precipitate was pelleted by centrifugation at 17,000*g* for 5 min at 4°C. The pellet was briefly washed with ice-cold labeling buffer A [0.1 M sodium phosphate (pH 6.8), 200 mM NaCl, 1 mM EDTA, 5% glycerol, and 0.2% Triton X-100] containing (NH$_4$)$_2$SO$_4$ at 70% of saturation. For complete removal of DTT, the washing step was repeated twice. The pellet was dissolved in 200 μl of labeling buffer to a final protein concentration of ~2 mg/ml. The fluorescent dye derivatives DY547P1-maleimide (donor) and DY647P1-maleimide (acceptor), purchased from Dyomics GmbH, were dissolved in dimethylformamide, added to the protein sample at an 8:1 (dye/protein) molar ratio, and incubated at room temperature for 1 hour, followed by overnight incubation at 4°C. The reaction was quenched by adding 0.5% (v/v) of β-mercaptoethanol. To remove the excess of unincorporated dyes, the protein was passed through 10-ml Sephadex G-25 glass column equilibrated with storage buffer [20 mM tris-HCl (pH 7.9), 300 mM NaCl, 0.5 mM EDTA, 0.2 mM β-mercaptoethanol, and 0.05% Triton X-100]. Labeling efficiency was calculated using the following equation: (moles dye per mole of protein) = $A_{dye}/(\varepsilon_{dye} \times C_{protein})$, where A_{dye} is the absorbance value of the dye at the absorption maximum, ε_{dye} is the molar extinction coefficient of the dye at the absorption maximum (ε_{Dy547} = 150,000 M^{-1} cm^{-1}; ε_{Dy647} = 250,000 M^{-1} cm^{-1}), and $C_{protein}$ is the σ subunit concentration in mole per liter. Labeling efficiencies of the σ^{70} subunit for donor and acceptor were ~94 and 45%, respectively. Labeling efficiencies of the σ^B subunit for donor and acceptor were ~80 and ~ 40%, respectively.

Run-off transcription, KMnO$_4$ probing, and EMSA
RNAP holoenzymes were reconstituted by mixing 100 nM core RNAP and 300 nM of the σ subunit in transcription buffer (TB) [20 mM tris-HCl (pH 7.9), 50 mM NaCl, 5 mM MgCl$_2$, 0.5 mM DTT, 0.1 mM EDTA, and 5% glycerol] and then incubating for 10 min at 37°C. When indicated, RbpA was used at 300 nM. The reaction mixtures were incubated with *sin*P3 and *sigA*P promoter DNA templates (40 nM) at 37°C for 10 min. Transcription was initiated by the addition of adenosine 5′-triphosphate, guanosine 5′-triphosphate, and cytidine 5′-triphosphate (to a final concentration of 25 μM each), 3 μCi of [α-^{32}P] uridine 5′-triphosphate (UTP) (PerkinElmer Life Sciences), and 1 μM UTP and was carried out for 5 min at 37°C. The transcription assays on *sigA*P were performed in the presence of 100 μM GpC primer (Eurogentec). For the order-of-addition experiments, RbpA was added to the reaction mixture either before DNA template or together with NTPs. Reactions were stopped by adding 1 volume of the stop solution (8 M urea and 20 mM EDTA). [^{32}P]RNA products were resolved on a 24% polyacrylamide gel electrophoresis (PAGE)/7 M urea denaturing gel. The KMnO$_4$ probing reactions were performed in 20-μl TB. RNAP holoenzymes were reconstituted by incubating 200 nM core RNAP and 600 nM of the σ subunit in TB for 10 min at 37°C. The *sigA*P promoter DNA fragment (40 nM) labeled by fluorescein at the 5′-end of template strand was added to the reactions and incubated for another 10 min at 37°C. The samples were treated with 5 mM KMnO$_4$ for 60 s and processed as described before (*32*). DNA fragments were analyzed on 10% PAGE/7 M urea sequencing gel. For the EMSA experiments, the synthetic fork junction DNA template (50 nM) was incubated with 100 nM RNAP, 300 nM σ subunit, and 300 nM RbpA in TB for 30 min at 22°C in the presence of poly(deoxyinosinic-deoxycytidylic acid) (10 μg/ml). For the order-of-addition experiments, RbpA was added to the reaction mixture either before us-fork DNA or after 5 min of incubation with us-fork DNA. Samples were resolved on 6% native 0.5 × tris-borate EDTA–PAGE. All gels were scanned by Typhoon 9200 Imager (GE Healthcare) and quantified using ImageQuant software.

smFRET sample preparation
The donor-acceptor–labeled σ^B subunit at 25 pM and the donor-acceptor–labeled σ^{70} subunit at 75 pM were prepared in the filtered (0.1 μm) FRET buffer [20 mM tris-HCl (pH 7.9), 150 mM NaCl, 5 mM MgCl$_2$, 5% glycerol, and bovine serum albumin (0.1 mg/ml)]. When indicated, ligands, *Mtb*RNAP core, *Eco*RNAP core, and RbpA were added to a final concentration of 500 nM. To reconstitute *Eco*RNAP-σ^{70} and *Mtb*RNAP-σ^B holoenzymes with and without RbpA, the samples were incubated at 37°C for 10 min. When indicated, us-fork DNA, either unlabeled or labeled with black hole quencher (BHQ2) at position −18 of the nontemplate DNA strand (Q-fork; fig. S6), was added to a final concentration of 500 nM and incubated for 10 min at room temperature. Complexes of *Mtb*RNAP with the *sigA*P promoter were formed in the FRET buffer containing 50 mM NaCl as described above and incubated at 37°C for 10 min before data acquisition. The *sigA*P promoter was added to a final concentration of 500 nM.

smFRET measurements and data analysis
smFRET measurements were performed on homebuilt confocal PIE-MFD microscope, as described (*17*). Samples were placed in transparent nonbinding 384-well plates (Corning), and acquisitions were performed for at least 3 hours at room temperature (22°C). Collected data were analyzed with the "Software Package for Multiparameter Fluorescence Spectroscopy, Full Correlation and Multiparameter Fluorescence

Imaging" developed in the C. A. M. Seidel laboratory (www.mpc.uni-duesseldorf.de/) (33). A single-molecule event was defined as a burst containing at least 30 photons. Further selection of the relevant species containing donor-acceptor was performed by selecting only the molecules satisfying the following criteria: (i) number of photons detected in the acceptor channel upon acceptor excitation >20, (ii) excited state lifetime of the acceptor upon acceptor excitation 0.55 ns < τ_A < 2.65 ns, and (iii) stoichiometry ratio $S > 0.4$ (fig. S1E) (34). Photobleached molecules were also eliminated using the methods described by Kudryavtsev et al. (18). For each photon burst, the apparent donor-acceptor FRET efficiencies (E_{PR}) were calculated as $E_{PR} = (I_A)/(I_D + I_A)$ (where I_A and I_D are intensities detected on the donor-acceptor channels) and plotted. For each identified subpopulation, donor excited lifetime analysis was used to calculate donor-acceptor smFRET efficiency (E) using the following equation: ($E = 1 - \tau_{DA}/\tau_D$), where τ_{DA} is the donor excited lifetime in the selected donor-acceptor subpopulation, and τ_D is the donor excited lifetime of the donor-only subpopulation. The E_{PR} histograms were analyzed using the OriginPro software. Most of the data were fitted with a sum of two or three Gaussian functions without fixing their center position or widths. The EcoRNAP-σ^{70} data were fitted with a sum of three Gaussian functions by fixing the width of the high FRET peak to 0.2.

Molecular brightness and FCS analysis

To verify that the RNAP holoenzyme assembled with the labeled σ subunit remained monomeric under our experimental conditions, we calculated the molecular brightness (MB) of the acceptor dye (which does not depend on the FRET efficiency) for each specific smFRET subpopulation. The analysis demonstrated that MB of the RNAP holoenzyme was identical to the one measured for the free σ subunit, suggesting that no oligomerization occurs upon holoenzyme assembly (fig. S3). For the ssFCS analysis, donor-acceptor cross-correlation curves on selected subspecies were fitted using the following model

$$G_{\mathrm{diff}}(t_c) = 1 + \frac{1}{N} \cdot \left(1 + \frac{t_c}{t_D}\right)^{-1} \cdot \left(1 + \left(\frac{\omega_0}{z_0}\right)^2 \cdot \frac{t_c}{t_D}\right)^{-\frac{1}{2}} \quad (1)$$

where N is the average number of molecules in the observation volume; t_D is the diffusion time; ω_0 and z_0 are the $1/e^2$ radii of the laser focus volume perpendicular to and along the optical axis, respectively; and t_c is the correlation time. FCS data were analyzed with the "Software Package for Multiparameter Fluorescence Spectroscopy, Full Correlation and Multiparameter Fluorescence Imaging" developed in the C. A. M. Seidel laboratory (33). No parameter was fixed during the fitting procedure.

smFRET distance calculations and molecular modeling

To determine accurate donor-acceptor distances (R_{DA}), we took advantage of the available crystal structures of RNAPs from E. coli, Thermus sp., and M. smegmatis in complex with promoter DNA (8, 9, 22, 35–37). In these structures, the mean distance between the donor and acceptor attachment points in σ^B (Cα atoms of Cys^{151} and Cys^{292}) is 69 ± 0.6 Å and between the donor and acceptor attachment points in σ^{70} (Cα atoms of Cys^{442} and Cys^{579}) is 60.7 ± 0.3 Å (tables S2 and S4). Real donor-acceptor distances should be different from the distances between dye attachment points due to the contribution of the linker, the fluorophore geometry, and constraints arising from steric clash of the dyes with pro-

tein and DNA. To take these factors into account, we modeled real donor-acceptor distance distribution in the crystal structures of the RNAP using FRET positioning and screening (FPS) software (fig. S4) (38). To model dye accessible volume (AV) clouds and dye position distributions for the σ^{70}-Cys^{442}-Cys^{579} derivative, we used atomic coordinates from the crystal structures of the E. coli RNAP holoenzyme (PDB code: 4IGC) and Thermus aquaticus RNAP in complex with us-fork DNA (PDB code: 4XLQ). To assess the effect of the us-fork DNA binding on R_{DA}, a model of E. coli RNAP with us-fork was built by fitting 4XLQ into 4IGC in UCSF Chimera software (39). We observed that the calculated R_{DA} distances were 4 to 7 Å shorter than the distances between Cα atoms of Cys^{442} and Cys^{579}. Addition of the us-fork DNA to E. coli RNAP restricted dye mobility and resulted in ~2 Å increase in R_{DA}. To model dye AV clouds and dye position distributions for the σ^B-Cys^{151}-Cys^{292} derivative, we used coordinates from a crystal structure of M. smegmatis RNAP in complex with us-fork DNA (PDB code: 5TW1). To assess the effect of the us-fork DNA binding on R_{DA}, us-fork DNA was removed from the structure. We observed that the calculated R_{DA} distances were 8 to 14 Å longer than the distances between Cα atoms of Cys^{151} and Cys^{292}. Addition of DNA restricted dye mobility and resulted in ~6 Å increase in R_{DA}. The FPS-calculated R_{DA} distances were used as reference in the following smFRET distance calculations. Using an experimental E value and R_{DA} calculated for these complexes, we calculated an "experimental" R_0 (R_0) as follows

$$R_0 = \frac{R_{DA}}{\left(\frac{1}{E} - 1\right)^{\frac{1}{6}}} \quad (2)$$

The R_0 values (indicated by asterisks in fig. S4) were used for the calculation of R for the other species of unknown structure (tables S2 and S3).

SUPPLEMENTARY MATERIALS

Supplementary material for this article is available at http://advances.sciencemag.org/cgi/content/full/4/5/eaao5498/DC1

fig. S1. Incorporation of the fluorescent dyes into σ^{70} and σ^B subunits.
fig. S2. Activity of the σ^{70} and σ^B double-Cys mutants and their labeled derivatives.
fig. S3. Test of protein oligomerization using MB analysis on the labeled species.
fig. S4. Calculation of the donor-acceptor distances using FPS software.
fig. S5. Analysis of the RNAP holoenzyme assembly by the ssFCS.
fig. S6. Interaction of RNAP with an us-fork template.
table S1. Apparent distances (R_{ap}) between domains $\sigma2$ and $\sigma4$ determined in ensemble LRET experiments.
table S2. Summary of the donor-acceptor distances for σ^{70} C442-C579.
table S3. Summary of the donor-acceptor distances for σ^B C151-C292.
Reference (40)

REFERENCES AND NOTES

1. A. Feklístov, B. D. Sharon, S. A. Darst, C. A. Gross, Bacterial sigma factors: A historical, structural, and genomic perspective. Annu. Rev. Microbiol. 68, 357–376 (2014).
2. A. J. Dombroski, W. A. Walter, C. A. Gross, Amino-terminal amino acids modulate σ-factor DNA-binding activity. Genes Dev. 7, 2446–2455 (1993).
3. A. J. Dombroski, W. A. Walter, M. T. Record Jr., D. A. Siegele, C. A. Gross, Polypeptides containing highly conserved regions of transcription initiation factor σ^{70} exhibit specificity of binding to promoter DNA. Cell 70, 501–512 (1992).
4. E. C. Schwartz, A. Shekhtman, K. Dutta, M. R. Pratt, D. Cowburn, S. Darst, T. W. Muir, A full-length group 1 bacterial sigma factor adopts a compact structure incompatible with DNA binding. Chem. Biol. 15, 1091–1103 (2008).
5. S. Callaci, E. Heyduk, T. Heyduk, Core RNA polymerase from E. coli induces a major change in the domain arrangement of the σ^{70} subunit. Mol. Cell 3, 229–238 (1999).
6. A. Feklistov, N. Barinova, A. Sevostyanova, E. Heyduk, I. Bass, I. Vvedenskaya, K. Kuznedelov, E. Merkienė, E. Stavrovskaya, S. Klimašauskas, V. Nikiforov, T. Heyduk,

K. Severinov, A. Kulbachinskiy, A basal promoter element recognized by free RNA polymerase σ subunit determines promoter recognition by RNA polymerase holoenzyme. *Mol. Cell* **23**, 97–107 (2006).

7. K. Kuznedelov L. Minakhin, A. Niedziela-Majka, S. L. Dove, D. Rogulja, B. E. Nickels, A. Hochschild, T. Heyduk, K. Severinov, A role for interaction of the RNA polymerase flap domain with the σ subunit in promoter recognition. *Science* **295**, 855–857 (2002).

8. K. S. Murakami, S. Masuda, E. A. Campbell, O. Muzzin, S. A. Darst, Structural basis of transcription initiation: An RNA polymerase holoenzyme-DNA complex. *Science* **296**, 1285–1290 (2002).

9. Y. Zuo, T. A. Steitz, Crystal structures of the *E. coli* transcription initiation complexes with a complete bubble. *Mol. Cell* **58**, 534–540 (2015).

10. R. M. Saecker, M. T. Record Jr., P. L. de Haseth, Mechanism of bacterial transcription initiation: RNA polymerase—Promoter binding, isomerization to initiation-competent open complexes, and initiation of RNA synthesis. *J. Mol. Biol.* **412**, 754–771 (2011).

11. Y. Hu, Z. Morichaud, S. Chen, J.-P. Leonetti, K. Brodolin, *Mycobacterium tuberculosis* RbpA protein is a new type of transcriptional activator that stabilizes the σ^A-containing RNA polymerase holoenzyme. *Nucleic Acids Res.* **40**, 6547–6557 (2012).

12. Y. Hu, Z. Morichaud, A. S. Perumal, F. Roquet-Baneres, K. Brodolin, *Mycobacterium* RbpA cooperates with the stress-response σ^B subunit of RNA polymerase in promoter DNA unwinding. *Nucleic Acids Res.* **42**, 10399–10408 (2014).

13. E. A. Hubin, A. Tabib-Salazar, L. J. Humphrey, J. E. Flack, P. D. B. Olinares, S. A. Darst, E. A. Campbell, M. S. Paget, Structural, functional, and genetic analyses of the actinobacterial transcription factor RbpA. *Proc. Natl. Acad. Sci. U.S.A.* **112**, 7171–7176 (2015).

14. A. Tabib-Salazar, B. Liu, P. Doughty, R. A. Lewis, S. Ghosh, M.-L. Parsy, P. J. Simpson, K. O'Dwyer, S. J. Matthews, M. S. Paget, The actinobacterial transcription factor RbpA binds to the principal sigma subunit of RNA polymerase. *Nucleic Acids Res.* **41**, 5679–5691 (2013).

15. A. Dey, A. K. Verma, D. Chatterji, Role of an RNA polymerase interacting protein, MsRbpA, from *Mycobacterium smegmatis* in phenotypic tolerance to rifampicin. *Microbiology* **156**, 873–883 (2010).

16. R. Manganelli, Sigma factors: Key molecules in *Mycobacterium tuberculosis* physiology and virulence. *Microbiol. Spectr.* **2**, MGM2-0007-2013 (2014).

17. L. Olofsson, S. Felekyan, E. Doumazane, P. Scholler, L. Fabre, J. M. Zwier, P. Rondard, C. A. M. Seidel, J.-P. Pin, E. Margeat, Fine tuning of sub-millisecond conformational dynamics controls metabotropic glutamate receptors agonist efficacy. *Nat. Commun.* **5**, 5206 (2014).

18. V. Kudryavtsev, M. Sikor, S. Kalinin, D. Mokranjac, C. A. M. Seidel, D. C. Lamb, Combining MFD and PIE for accurate single-pair Förster resonance energy transfer measurements. *ChemPhysChem* **13**, 1060–1078 (2012).

19. S. Felekyan, S. Kalinin, H. Sanabria, A. Valeri, C. A. M. Seidel, Filtered FCS: Species auto- and cross-correlation functions highlight binding and dynamics in biomolecules. *ChemPhysChem* **13**, 1036–1053 (2012).

20. Y. Guo, J. D. Gralla, Promoter opening via a DNA fork junction binding activity. *Proc. Natl. Acad. Sci. U.S.A.* **95**, 11655–11660 (1998).

21. A. Bortoluzzi, F. W. Muskett, L. C. Waters, P. W. Addis, B. Rieck, T. Munder, S. Schleier, F. Forti, D. Ghisotti, M. D. Carr, H. M. O'Hare, *Mycobacterium tuberculosis* RNA polymerase-binding protein A (RbpA) and its interactions with sigma factors. *J. Biol. Chem.* **288**, 14438–14450 (2013).

22. E. A. Hubin, A. Fay, C. Xu, J. M. Bean, R. M. Saecker, M. S. Glickman, S. A. Darst, E. A. Campbell, Structure and function of the mycobacterial transcription initiation complex with the essential regulator RbpA. *eLife* **6**, e22520 (2017).

23. A. Kumar, R. A. Malloch, N. Fujita, D. A. Smillie, A. Ishihama, R. S. Hayward, The minus 35-recognition region of *Escherichia coli* sigma 70 is inessential for initiation of transcription at an "extended minus 10" promoter. *J. Mol. Biol.* **232**, 406–418 (1993).

24. S. Tagami, S.-i Sekine, L. Minakhin, D. Esyunina, R. Akasaka, M. Shirouzu, A. Kulbachinskiy, K. Severinov, S. Yokoyama, Structural basis for promoter specificity switching of RNA polymerase by a phage factor. *Genes Dev.* **28**, 521–531 (2014).

25. A. Chakraborty, D. Wang, Y. W. Ebright, Y. Korlann, E. Kortkhonjia, T. Kim, S. Chowdhury, S. Wigneshweraraj, H. Irschik, R. Jansen, B. T. Nixon, J. Knight, S. Weiss, R. H. Ebright, Opening and closing of the bacterial RNA polymerase clamp. *Science* **337**, 591–595 (2012).

26. S. A. Darst, N. Opalka, P. Chacon, A. Polyakov, C. Richter, G. Zhang, W. Wriggers, Conformational flexibility of bacterial RNA polymerase. *Proc. Natl. Acad. Sci. U.S.A.* **99**, 4296–4301 (2002).

27. T. Cortes, O. T. Schubert, G. Rose, K. B. Arnvig, I. Comas, R. Aebersold, D. B. Young, Genome-wide mapping of transcriptional start sites defines an extensive leaderless transcriptome in *Mycobacterium tuberculosis*. *Cell Rep.* **5**, 1121–1131 (2013).

28. Z. Morichaud, L. Chaloin, K. Brodolin, Regions 1.2 and 3.2 of the RNA polymerase σ subunit promote DNA melting and attenuate action of the antibiotic lipiarmycin. *J. Mol. Biol.* **428** (2 Pt. B), 463–476 (2016).

29. N. Zenkin, A. Kulbachinskiy, Y. Yuzenkova, A. Mustaev, I. Bass, K. Severinov, K. Brodolin, Region 1.2 of the RNA polymerase σ subunit controls recognition of the −10 promoter element. *EMBO J.* **26**, 955–964 (2007).

30. S. P. Haugen, W. Ross, M. Manrique, R. L. Gourse, Fine structure of the promoter-σ region 1.2 interaction. *Proc. Natl. Acad. Sci. U.S.A.* **105**, 3292–3297 (2008).

31. Y. Kim, S. O. Ho, N. R. Gassman, Y. Korlann, E. V. Landorf, F. R. Collart, S. Weiss, Efficient site-specific labeling of proteins via cysteines. *Bioconjug. Chem.* **19**, 786–791 (2008).

32. A. Tupin, M. Gualtieri, J.-P. Leonetti, K. Brodolin, The transcription inhibitor lipiarmycin blocks DNA fitting into the RNA polymerase catalytic site. *EMBO J.* **29**, 2527–2537 (2010).

33. J. Widengren, V. Kudryavtsev, M. Antonik, S. Berger, M. Gerken, C. A. M. Seidel, Single-molecule detection and identification of multiple species by multiparameter fluorescence detection. *Anal. Chem.* **78**, 2039–2050 (2006).

34. A. N. Kapanidis, N. K. Lee, T. A. Laurence, S. Doose, E. Margeat, S. Weiss, Fluorescence-aided molecule sorting: Analysis of structure and interactions by alternating-laser excitation of single molecules. *Proc. Natl. Acad. Sci. U.S.A.* **101**, 8936–8941 (2004).

35. K. S. Murakami, X-ray crystal structure of *Escherichia coli* RNA polymerase σ^70 holoenzyme. *J. Biol. Chem.* **288**, 9126–9134 (2013).

36. Y. Zuo, Y. Wang, T. A. Steitz, The mechanism of *E. coli* RNA polymerase regulation by ppGpp is suggested by the structure of their complex. *Mol. Cell* **50**, 430–436 (2013).

37. B. Bae, A. Feklistov, A. Lass-Napiorkowska, R. Landick, S. A. Darst, Structure of a bacterial RNA polymerase holoenzyme open promoter complex. *eLife* **4**, e08504 (2015).

38. S. Kalinin, T. Peulen, S. Sindbert, P. J. Rothwell, S. Berger, T. Restle, R. S. Goody, H. Gohlke, C. A. M. Seidel, A toolkit and benchmark study for FRET-restrained high-precision structural modeling. *Nat. Methods* **9**, 1218–1227 (2012).

39. E. F. Pettersen, T. D. Goddard, C. C. Huang, G. S. Couch, D. M. Greenblatt, E. C. Meng, T. E. Ferrin, UCSF Chimera—A visualization system for exploratory research and analysis. *J. Comput. Chem.* **25**, 1605–1612 (2004).

40. The PyMOL Molecular Graphics System, Version 1.8 Schrödinger, LLC.

Citation: R. K. Vishwakarma, A.-M. Cao, Z. Morichaud, A. S. Perumal, E. Margeat, K. Brodolin, Single-molecule analysis reveals the mechanism of transcription activation in *M. tuberculosis*. *Sci. Adv.* **4**, eaao5498 (2018).

Science Advances

Single-molecule analysis reveals the mechanism of transcription activation in *M. tuberculosis*

Rishi Kishore Vishwakarma, Anne-Marinette Cao, Zakia Morichaud, Ayyappasamy Sudalaiyadum Perumal, Emmanuel Margeat and Konstantin Brodolin

ARTICLE TOOLS	http://advances.sciencemag.org/content/4/5/eaao5498
SUPPLEMENTARY MATERIALS	http://advances.sciencemag.org/content/suppl/2018/05/21/4.5.eaao5498.DC1
REFERENCES	This article cites 39 articles, 14 of which you can access for free http://advances.sciencemag.org/content/4/5/eaao5498#BIBL
PERMISSIONS	http://www.sciencemag.org/help/reprints-and-permissions

Use of this article is subject to the Terms of Service